molecular pharmaceutics

Article

pubs.acs.org/molecularpharmaceutics

Effects of Membrane PEGylation on Entry and Location of Antifungal Drug Itraconazole and Their Pharmacological Implications

Monika Dzieciuch-Rojek,[†,∥] Chetan Poojari,[‡,∥] Jan Bednar,[§,¶] Alex Bunker,[‡‡] Bartłomiej Kozik,[†] Maria Nowakowska,[†] Ilpo Vattulainen,[‡,∇,&] Paweł Wydro,[†] Mariusz Kepczynski,*[,†] and Tomasz Róg*[,‡,∇]

[†]Faculty of Chemistry, Jagiellonian University, Ingardena 3, 30-060 Kraków, Poland

[‡]Department of Physics, Tampere University of Technology, P.O. Box 692, FI-33101 Tampere, Finland

[§]Université de Grenoble Alpes/CNRS, Institut Albert Bonniot, UMR 5309, 38042 CEDEX 9 Grenoble, France

[¶]First Faculty of Medicine, Laboratory of Biology and Pathology of the Eye, Institute of Inherited Metabolic Disorders, Charles University in Prague, KeKarlovu 2, 12800 Prague 2, Czech Republic

[‡‡]Centre for Drug Research, Division of Pharmaceutical Biosciences, Faculty of Pharmacy, University of Helsinki, FI-00014 Helsinki, Finland

[∇]Department of Physics, University of Helsinki, P.O. Box 64, FI-00014 Helsinki, Finland

[&]MEMPHYS—Center for Biomembrane Physics, University of Southern Denmark, Odense, Denmark

Supporting Information

ABSTRACT: Itraconazole (ITZ) is an antifungal agent used clinically to treat mycotic infections. However, its therapeutic effects are limited by low solubility in aqueous media. Liposome-based delivery systems (LDS) have been proposed as a delivery mechanism for ITZ to alleviate this problem. Furthermore, PEGylation, the inclusion in the formulation of a protective "stealth sheath" of poly(ethylene glycol) around carrier particles, is widely used to increase circulation time in the bloodstream and hence efficacy. Together, these themes highlight the importance of mechanistic and structural understanding of ITZ incorporation into liposomes both with and without PEGylation because it can provide a potential foundation for the rational design of LDS-based systems for delivery of ITZ, using alternate protective polymers or formulations. Here we have combined atomistic simulations, cryo-TEM, Langmuir film balance, and fluorescence quenching experiments to explore how ITZ interacts with both pristine and PEGylated liposomes. We found that the drug can be incorporated into conventional and PEGylated liposomes for drug concentrations up to 15 mol % without phase separation. We observed that, in addition to its protective properties, PEGylation significantly increases the stability of liposomes that host ITZ. In a 1-palmitoyl-2-oleoyl-*sn*-glycero-3-phosphocholine (POPC) bilayer without PEGylation, ITZ was found to reside inside the lipid bilayer between the glycerol and the double-bond regions of POPC, adopting a largely parallel orientation along the membrane surface. In a PEGylated liposome, ITZ partitions mainly to the PEG layer. The results provide a solid basis for further development of liposome-based delivery systems.

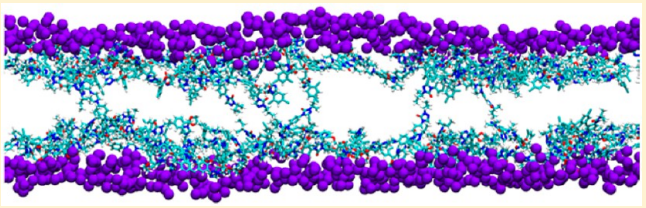

KEYWORDS: *lipid bilayer, itraconazole, sterically stabilized liposomes, cryo-TEM, polyethylene glycol (PEG), molecular dynamics simulations*

1. INTRODUCTION

The drug itraconazole (ITZ, Figure 1) is an orally administered triazole antifungal agent that has been approved, and is widely used, to treat serious mycotic infections in both normal and immunocompromised patients.[1] It acts as an inhibitor of the enzyme lanosterol 14 α-demethylase, a member of the cytochrome P450 family. The mechanism of antifungal activity involves impairment of the synthesis of ergosterol, an essential ingredient of the fungal cell membranes.[2] Additionally, the principal metabolite of ITZ, hydroxyl-itraconazole (OH-itraconazole), also exhibits antifungal activity at a level comparable to that of ITZ itself.[3] Additionally, ITZ has been proposed as a potent inhibitor for P-glycoprotein that is a multidrug resistant protein in tumor cells.[4]

The therapeutic effect of ITZ is, however, limited by its low solubility in aqueous media, reaching approximately 1 ng/mL at neutral pH and less than 5 μg/mL in diluted acidic solutions.[5] As is the case for all drug molecules, solubility and dissolution rates are critical parameters that determine absorption

Received: October 26, 2016
Revised: January 25, 2017
Accepted: February 24, 2017
Published: February 24, 2017

DOI: 10.1021/acs.molpharmaceut.6b00969
Mol. Pharmaceutics 2017, 14, 1057−1070

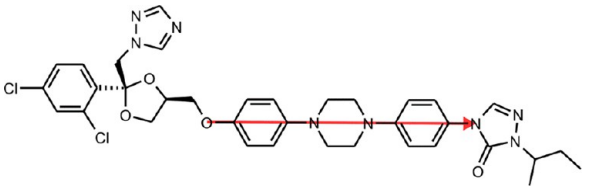

Figure 1. Structure of a (2*R*,4*S*) stereoisomer of itraconazole (ITZ) depicting the vector (red arrow) of its principal axis that defines the molecule's key orientation.

efficiency at the target site and thus drug efficacy.[6] In several cases, ITZ must be formulated for intravenous delivery, particularly for the neutropenic and other immunocompromised patients, who, as a result, have difficulty swallowing the oral delivery formulation of the drug.[7] Various techniques have been developed to enhance ITZ solubility in aqueous media.[8−11] One of the most common methods for increasing solubility of poorly water-soluble drugs is inclusion into the cavity of cyclodextrins. The only commercially available intravenous formulation of ITZ is SPORANOX I.V., where the drug is solubilized by the adjuvant hydroxypropyl-cyclodextrin (HP-CD).[12] Unfortunately, the use of SPORANOX has not been approved for patients with impaired renal function because of toxicity issues related to the HP-CD adjuvant.[13]

Phospholipid liposomes can be considered as more attractive, nontoxic alternative carriers. Liposomes are spherical vesicles composed of amphiphilic lipids, such as phosphatidylcholines or ceramides. They are used as models of biological membranes in studies of passive drug uptake.[14,15] Moreover, since the 1970s, liposomes have been used as systems for drug delivery.[16,17] Most frequently, liposomes are formulated from lipids naturally occurring in biomembranes; however, synthetic and specifically designed lipids have become a common alternative.[18,19] They are versatile carriers capable of carrying hydrophobic drugs within the membrane[20] or a payload of hydrophilic drugs in the aqueous interior.[21] Unfortunately, once in the bloodstream, liposomes are vulnerable to uptake by the mononuclear phagocyte system (MPS).[22] The process involves first a specific cascade of proteins of the complement system that adhere to the liposome surface in a process known as opsonization.[23] This signals for removal of the liposome from the blood circulation by macrophages in the liver and spleen.[24,25] Thus, liposomes have a circulation half-life in the bloodstream of only ∼1 h, which limits bioavailability and efficacy of the drug payload. Incorporation of lipids with covalently attached poly(ethylene glycol) (PEG) chains into the liposome increases the stability of vesicle dispersions and inhibits elimination of the liposomes from the bloodstream. While the exact mechanism remains unclear, the benefit is clear: circulation half-life is increased to 1−2 days.[24] Such vesicles are known as PEGylated or sterically stabilized liposomes (SSLs) and are used as effective drug delivery systems.[26] While other possible polymers can be used to form the protective shell on liposomes, PEG is currently the gold standard, as it possesses some unique properties beneficial for this application. In particular, PEG is soluble in typical organic solvents in addition to water,[27] nontoxic, and eliminated from the body through a combination of renal and hepatic pathways.[28] Furthermore, PEG possesses one of the lowest levels of protein or cellular absorption among any known polymers. These unusual properties of PEG may be explained by high hydration of the polyether backbone of PEG.

Several liposome-based formulations of ITZ have been developed. Recently, ITZ was efficiently (up to 80%) incorporated into multilamellar liposomes composed of dipalmitoylphosphatidylcholine (DPPC) and cholesterol and administered intravenously into mice.[29] The delivery of ITZ in this form increased the drug concentration in infected tissues, thus improving its in vivo efficacy. Effectiveness of that formulation in treatment for pneumonia was greatly enhanced in comparison to that obtained when ITZ was administered intravenously in the cyclodextrin carrier or orally (dissolved in PEG).[30] ITZ-loaded liposomes coated with carboxymethylchitosan were shown to have a longer elimination time in comparison to the equivalent uncoated liposomes.[31] After intravenous injection, the system demonstrated high targeting efficiency toward the lungs. Additionally, the solubilized ITZ preserved its antifungal activity.

Although the initial in vivo results for the liposomal ITZ intravenous delivery systems are quite promising, very little is known about the physicochemical properties of these systems. Here we explore this complicated topic through a number of experimental techniques (Langmuir film balance, cryo-transmission electron microscopy (cryo-TEM), and fluorescence quenching experiments) combined with computational atomistic molecular dynamics (MD) simulations. This multidisciplinary approach is largely the method of choice for unraveling nanoscale phenomena in biomolecular systems and previous applications of this approach have been highly successful in generating new knowledge for the development of liposome-based drug delivery systems.[17,28,32−35]

In this spirit, here we consider ITZ accumulation in conventional as well as PEGylated liposomes, with particular attention paid to the influence of varying ITZ concentration on its binding to the liposomes and the consequent effects on lipid membrane properties. The main aim is to obtain mechanistic insight for the solubility and location of ITZ in a lipid bilayer and for the interplay of ITZ with lipid monolayers and bilayers.

2. EXPERIMENTAL SECTION

2.1. Materials. Synthetic 1-palmitoyl-2-oleoyl-*sn*-glycero-3-phosphocholine (POPC) and itraconazole (ITZ) were obtained from Sigma-Aldrich. *N*-[Carbonyl-methoxy(polyethylene glycol)-2000)-1,2-distearoyl-*sn*-glycero-3-phosphoethanolamine, sodium salt (DSPE-PEG) was acquired from NOF Europe (Belgium) NV. All solvents were of spectroscopy grade and purchased from POCH (Gliwice, Poland). Milli-Q water from a Millipore purification system was used in all experiments.

2.2. Apparatus. A Hewlett-Packard 8452A diode-array spectrophotometer equipped with a HP 89090A Peltier temperature control accessory was used to measure UV−vis absorption spectra at 25 °C. An SLM-AMINCO 8100 spectrofluorimeter with a thermostated cuvette holder was used to record steady-state fluorescence spectra at 25 °C. Emission spectra were corrected for the wavelength dependence of the detector response through use of an internal correction function provided by the manufacturer.

2.3. Langmuir Monolayer Measurements. The interactions between ITZ and POPC monolayer were studied using Langmuir balance measurements and Brewster angle microscopy (BAM). The Π-A isotherms were measured using a NIMA (U.K.) Langmuir trough (total area = 300 cm^2) as

DOI: 10.1021/acs.molpharmaceut.6b00969
Mol. Pharmaceutics 2017, 14, 1057−1070

described previously.[36] Stock solutions of POPC and DSPE-PEG were prepared in a chloroform/methanol 4:1 (v/v) mixture, whereas ITZ was dissolved in chloroform. The PBS solution of pH 7.4 formed the subphase, and its temperature was kept at 37 ± 0.1 °C using a thermostat. Spreading solutions of phospholipids were prepared in a chloroform/methanol 4:1 (v/v) mixture, whereas ITZ was dissolved in chloroform. The monolayers were compressed with a barrier speed of 20 cm^2/min in all experiments. The isotherms for each of the investigated monolayers were recorded at least twice, each time from a freshly prepared mixture. The reproducibility of the results was at least ±0.1 mN/m and ±0.2 nm^2/molecule.

2.4. Preparation of Small Unilamellar Liposomes (SUVs). Pure POPC and POPC/DSPE-PEG (7 mol % of PEGylated lipid) liposomes were prepared using a sonication method.[37] Briefly, POPC and POPC/DSPE-PEG were dissolved in chloroform and ethanol, respectively. Appropriate volumes of the solutions were placed in a volumetric flask, and the organic solvents were evaporated under nitrogen flow. The dry lipid film was hydrated by addition of appropriate volume of a 10 mM phosphate buffer of pH 7.4 to reach a POPC concentration of 2.5 mg/mL.

2.5. Cryo-Transmission Electron Microscopy (cryo-TEM). The Morphology of liposomes was observed using a cryo-TEM technique according to the procedure described elsewhere.[36] Liposomal dispersions were applied on a C-flat CF-4/2−2C electron microscopy grid previously activated with a glow discharge (10 mA for 30 s and 2×10^{-2} mbar).

2.6. Fluorescence Quenching Experiments. The POPC and POPC/DSPE-PEG liposomes with embedded ITZ (c_{ITZ} = 1.8 μM) were used in fluorescence quenching studies. The dispersion was placed in a cuvette, and increasing amounts of potassium iodide solution (c_{KI} = 1 M) were added. After each addition of quencher, the solution was equilibrated for 10 min, and emission spectra were measured with an excitation wavelength of 270 nm.

2.7. Atomistic MD Simulations. In a nutshell, MD simulations of a number of systems were performed (see Table 1). Images of initial and final system configurations are shown in Figures 2 and 3. As a control, we simulated a pure POPC bilayer without ITZ or PEGylation (system M0). We next studied the PEG-free system by means of a POPC bilayer hosting several ITZ molecules positioned at different initial locations. In system M1, a single ITZ molecule was initially positioned in the water phase (Figure 2). Systems M2, M3, and M4 contained 3 mol %, 9.1 mol %, and 16.6 mol % of ITZ molecules, in respective order, partially inserted into the lipid bilayer (see Figure 3). Finally, we considered the role of PEG in system M5, where we explored the POPC bilayer with ∼7 mol % of DSPE-PEG interacting with six ITZ molecules that were inserted into the aqueous phase between PEG chains (Figure 2). The ITZ molecule has four stereoisomers.[38] Due to computational limitations, we considered only the (2*R*,4*S*) stereoisomer (Figure 1).

Table 1. Summary of the Simulated Systems[a]s

system	ITZ	POPC	DSPE-PEG	water	Na^+/Cl^-	simulation length (ns)
M0	0	128	-	7077	37/37	1000
M1	1	128	-	7077	37/37	4 × 1000
M2	8	256	-	10835	30/30	1 × 350
M3	102	1024	-	83750	227/227	1 × 500
M4	204	1024	-	83750	227/227	1 × 500
M5	6	464	36	46782	267/231	2 × 1000

[a]The table indicates the number of molecules in the given system, the simulated time, and the number of repeats started from distinct initial condition.

To parametrize all lipid molecule types, ITZ, PEG, and ions, we employed the all-atom OPLS force field.[39] Details regarding force field implementation and choice of the partial charges can be found from our previously published work.[40−42] For water, we used the TIP3P model compatible with the all-atom OPLS-AA force field.[43] Partial charges for ITZ were derived according to the OPLS-AA methodology. Briefly, the charges were derived for smaller molecular fragments (see Figure S1 in Supporting Information (SI)) with flanking methyl groups added. The structure of each fragment was first optimized at the B3LYP/aug-cc-pVDZ level. Next, the electrostatic potential surrounding the fragment was calculated. These calculations were carried out using the Gaussian09 package.[44] Finally, the partial atomic charges were computed using the RESP program.[45] Derived charges are given in SI as a part of ITZ topology in a GROMACS format, generated using an MKTOP script.[46]

After solvating the systems with the TIP3P water model, 0.15 M NaCl salt was added to describe the system close to its physiological salt concentration. Prior to equilibration, the energy of the initial configurations was minimized by the steepest-descent algorithm. An initial equilibration was carried out under NVT conditions for 1 ns, and the v-rescale method was used to regulate the temperature at 300 K with a time constant of 0.1 ps.[47] During equilibration, IZT and the phosphorus atom of the lipid headgroups was restrained with a force constant of 1000 kJ mol^{-1} nm^{-2}. The systems were then equilibrated under NpT conditions for 10 ns and the Nosé−Hoover thermostat was used with a time constant of 0.5 ps to control the temperature. Pressure was regulated using the semi-isotropic Parrinello−Rahman barostat[48] using a reference pressure of 1 bar. For long-range Coulomb interactions, the particle-mesh Ewald (PME) method was used.[49] The linear constraint solver (LINCS) algorithm was used to preserve covalent bond lengths.[50] For the actual MD simulations, all restraints were removed from the system and the parameter settings were similar to those used during NpT equilibration. The time step for integration was set to 2 fs. All simulations were carried out using the GROMACS 4.6 software package.[51]

3. RESULTS

3.1. Monolayer Experiments Show That the Effects of ITZ on Pristine Lipid Monolayers Are Strongly ITZ Concentration-Dependent Unlike in PEGylated Monolayers, Where the Influence of ITZ Is Weak. Miscibility of the drug and phospholipids in a hydrated bilayer is of fundamental importance for effective embedding of hydrophobic drugs into liposomes. Lipid monolayers are considered as quite suitable models for studying miscibility of lipids in membranes. Therefore, we first investigated the interaction between ITZ and lipids in monolayers. Surface pressure−area (π−A) isotherms measured during the compression of one-component (POPC and ITZ) films, and their mixtures of various compositions are shown in Figure 4A. Figure 4B depicts the results for the systems containing the PEGylated lipid.

For the pure POPC monolayer, the value of π starts to rise as a mean molecular area of approximately 1.05 nm^2 is reached.

DOI: 10.1021/acs.molpharmaceut.6b00969
Mol. Pharmaceutics 2017, 14, 1057−1070

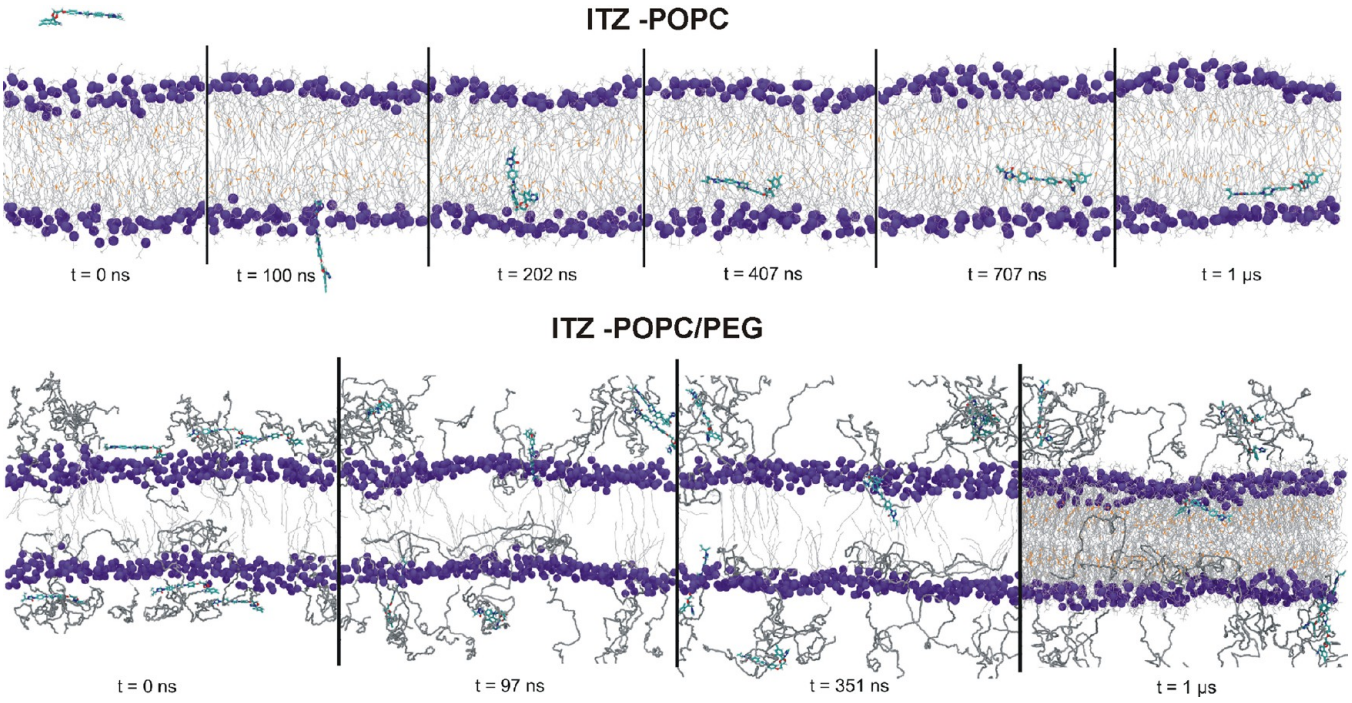

Figure 2. Snapshots of simulated systems containing ITZ, describing different states during the simulations: a POPC bilayer (system M1, top) and a POPC/DSPE-PEG mixture (system M5). The ITZ molecules are depicted as licorice and colored according to atom type. The POPC and DSPE molecules are depicted as light gray sticks, with purple spheres for phosphate groups. The PEG chains and double bonds are shown as gray licorice and orange sticks, respectively. For clarity, water and ions are not shown. All images were prepared using VMD.[52]

Further compression of the monolayer caused a gradual increase in the surface pressure up to π = 46 mN/m, corresponding to an area per molecule of ca. 0.64 nm^2, at which the monolayer collapses. The values of the compression modulus calculated for the POPC film (see Figure s2) show that it is in the liquid-condensed (LC) state at larger surface pressures. For the ITZ film, the increase of π occurs at a much larger area (ca. 2 nm^2/molecule) compared to the POPC monolayer. Moreover, the surface pressure is almost constant ($\pi \sim$ 5 mN/m) in the area region of 0.4−1.2 nm^2/molecule. The presence of such a plateau may correspond to a phase transition in the monolayer. The origin of this plateau is discussed below on the basis of the BAM results. For the case of mixed monolayers, the addition of a small amount of ITZ ($X_{ITZ} \leq 0.15$) to the POPC film moved the isotherms toward smaller areas, which is likely due to a different orientation of ITZ molecules in the mixed films in comparison to their orientation in a pure ITZ film, in which the molecules most likely lie flat on the surface. However, their shapes are very similar to that obtained for the pure phospholipid monolayer. A further increase in the ITZ content in the mixture ($X_{ITZ} \geq 0.2$) results in the appearance of an inflection in the isotherms. With an increase in the ITZ mole fraction, the inflection occurs at a lower surface pressure and gradually becomes longer and longer until finally reaching a region with a relatively constant surface pressure (pseudo plateau).

For the POPC/DSPE-PEG monolayer, we observed a starting pressure of approximately 1.5 mN/m. As indicated by the values of the compression modulus (Figure s2), the mixed film is initially in the liquid-expanded (LE) phase, in which the pressure is low and the surface layer is highly compressible. The presence of the LE phase at the beginning of the isotherm is a result of the spreading of the PEGylated lipids and formation of a thin layer covering the surface evenly. Subsequently, π rises slowly during the compression, then levels off forming a plateau at a value of ∼13 mN/m before growing rapidly to the A value of ∼0.8 nm^2. The presence of the plateau in the isotherm probably corresponds to the desorption of PEG chains from the air−water interface into the aqueous subphase. The steep pressure increase is a result of the system entering the liquid-condensed (LC) phase when the PEG chains are expelled from the interface (Figure s2). The isotherm shape obtained for the POPC/DSPE-PEG monolayer is in good agreement with those previously observed for various PC/PE−PEG systems.[28,53] The incorporation of ITZ to the POPC/DSPE-PEG film generally shifts the isotherms toward smaller areas; however, it had little effect on the polymer desorption into the subphase because the plateau length is almost the same for all ITZ mole fractions used in experiment. Moreover, the appearance of an inflection in the isotherms at the higher surface pressure is observed for $X_{ITZ} \geq 0.15$.

Deeper insight into the structure of the films was obtained using BAM microscopy. BAM images captured during compression of the POPC/ITZ and POPC/DSPE-PEG/ITZ mixed films are presented in Figures 5 and 6. For the pure POPC monolayer, features characteristic for the coexistence of a liquid-expanded and gaseous phases are observed at large molecular areas at π = 0 mN/m. With monolayer compression, the gaseous phase (dark structures) disappears as the film becomes homogeneous up to the collapse surface pressure. In contrast, for the case of the ITZ film, bright oval domains start to appear at the molecular area of 1.2 nm^2 ($\pi \sim$ 4.5 mN/m) corresponding to the beginning of the plateau in the isotherm. During the film compression these domains grow and then begin to merge with each other, causing a sharp increase in the surface pressure. Very high brightness of these domains may indicate that they are multilayer structures. Thus, ITZ is able to form a monomolecular film only at large molecular areas and

DOI: 10.1021/acs.molpharmaceut.6b00969
Mol. Pharmaceutics 2017, 14, 1057−1070

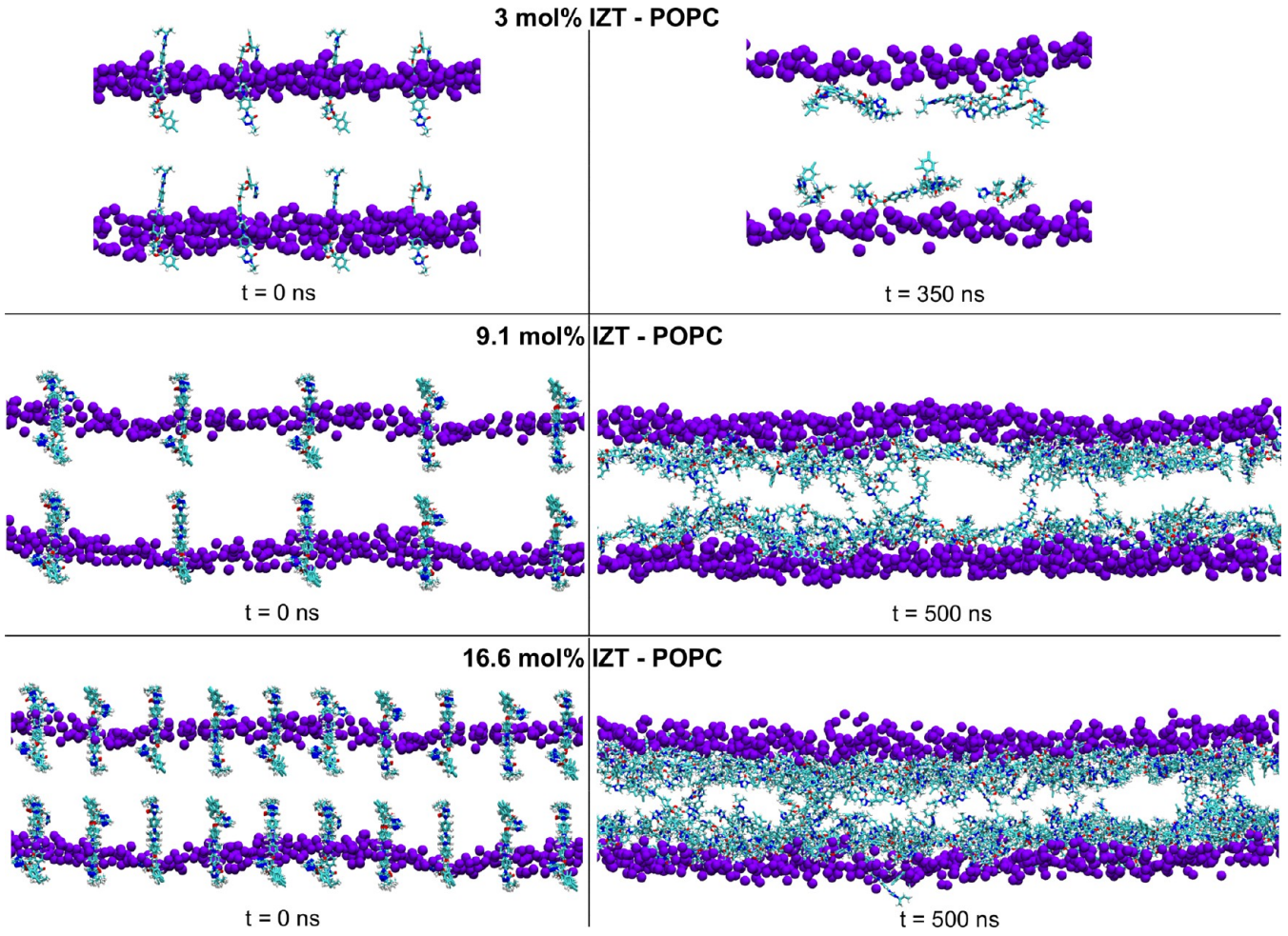

Figure 3. Snapshots of initial (left) and final (right) configurations of the systems M2 (top panels), M3 (middle panels), and M4 (lower panels). Lipid phosphate atoms are shown as purple spheres. The ITZ molecules are shown as licorice and colored according to atom type. For clarity, water, ions, and lipid hydrocarbon chains are not shown.

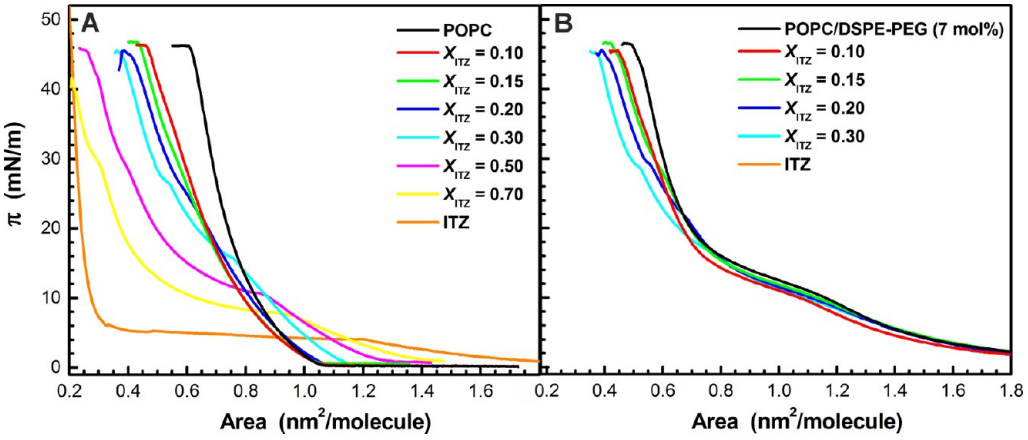

Figure 4. Selected surface pressure (π)−area isotherms for (A) the POPC/ITZ and (B) POPC/DSPE-PEG/ITZ monolayers measured at 37 °C. X_{ITZ} stands for the mole fraction of ITZ. The isotherm obtained for pure ITZ (orange line) is shown in panel A.

very low surface pressures. The compression of this film causes the transition of the monolayer into multilayer structures, which corresponds to the plateau in the π−A curve. Similar surface behavior, that is, the transition from a monolayer to a multilayer, was also found (e.g., for 4−octyl−4′−cyanobiphenyl).[54] For the case of the POPC monolayers containing up to 15 mol % of ITZ, the BAM images are practically the same as those obtained for the POPC film. The morphology of the mixed films changes when the mole fraction of ITZ is increased. For the monolayer with X_{ITZ} = 0.2, small bright spots can be observed at π = 25 mN/m. This corresponds to an inflection in the isotherm. The further increase of the ITZ content causes the bright structures to become larger and to appear at a lower surface pressure, which is highlighted as a drop of the transition

DOI: 10.1021/acs.molpharmaceut.6b00969
Mol. Pharmaceutics 2017, 14, 1057−1070

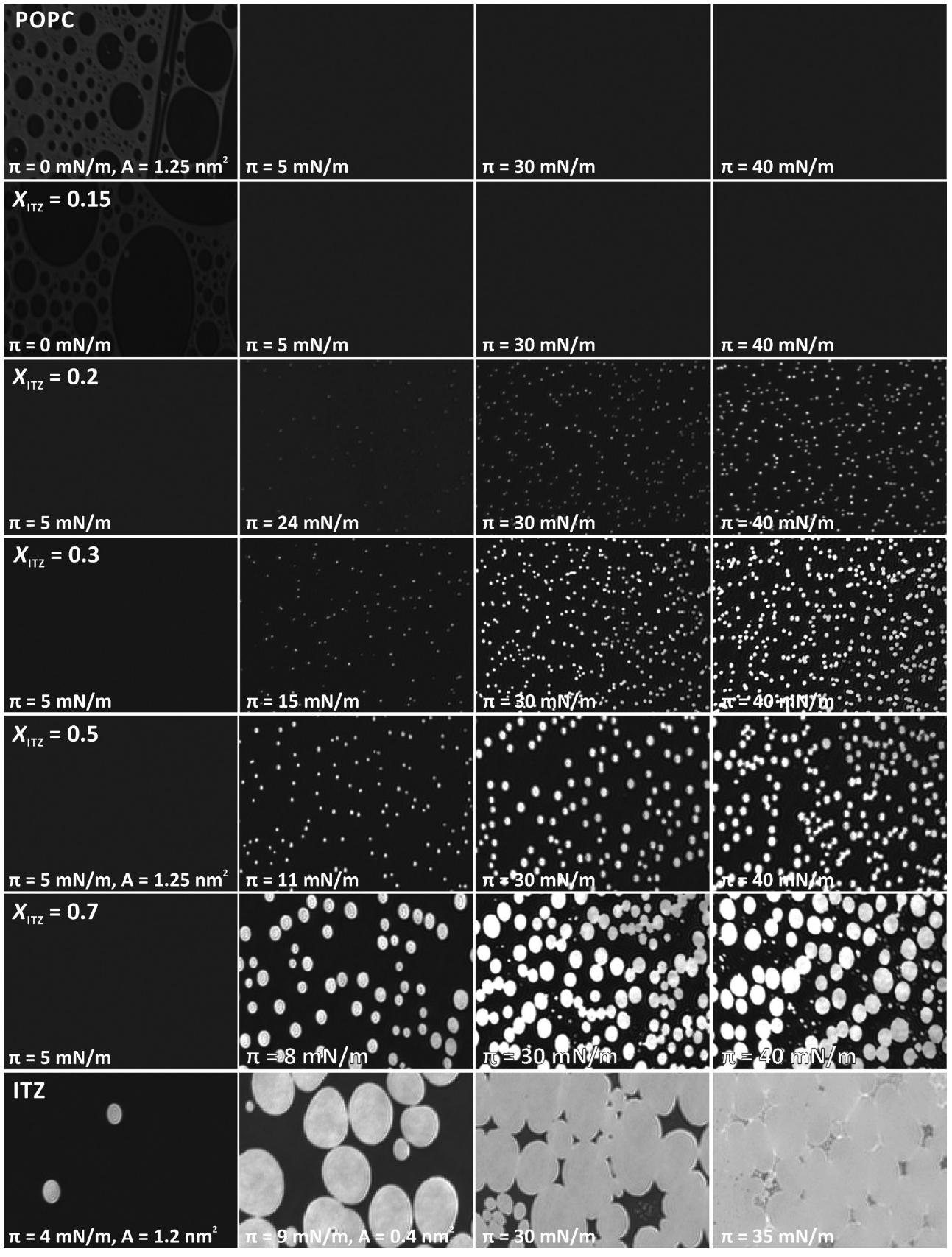

Figure 5. Brewster angle microscopy (BAM) pictures of the POPC/ITZ monolayers that were taken at different stages of film compression at 37 °C.

pressure due to the increase of the ITZ mole fraction. The films comprised of POPC/DSPC-PEG alone and with 10 mol % of ITZ were found to be homogeneous up to the collapse in surface pressure (Figure 6). The film with X_{ITZ} = 0.15 was

DOI: 10.1021/acs.molpharmaceut.6b00969
Mol. Pharmaceutics 2017, 14, 1057−1070

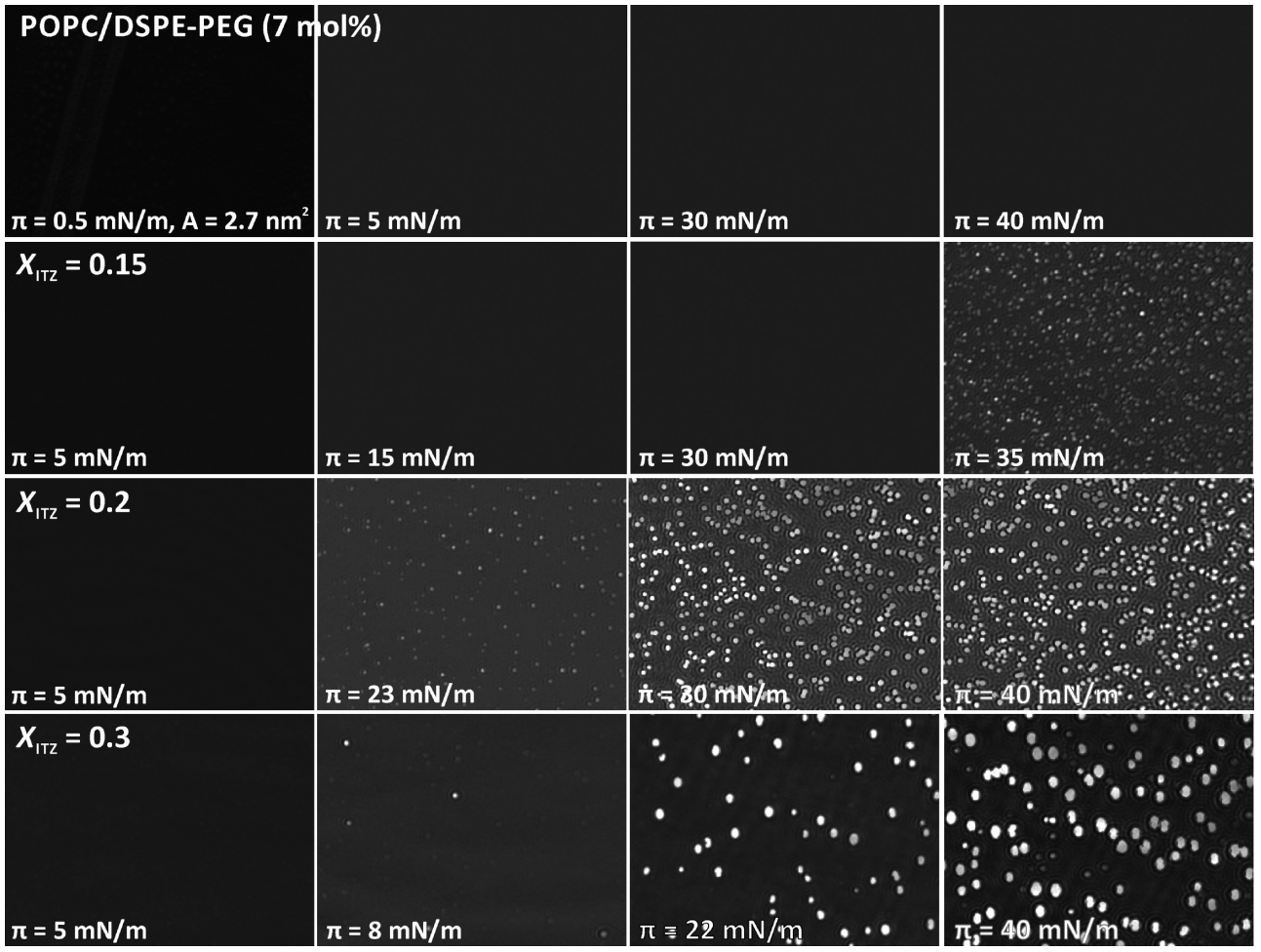

Figure 6. Brewster angle microscopy (BAM) pictures of the POPC/DSPE-PEG/ITZ monolayers that were taken at different stages of film compression at 37 °C.

homogeneous up to π = 30 mN/M, with small bright spots observed for higher surface pressures. Starting from X_{ITZ} = 0.20, the bright oval features become larger and appear at the lower values of π.

The results from the π−area isotherms and BAM microscopy show that the POPC monolayers containing up to 15 mol % of ITZ are completely homogeneous up to the collapse pressure, which indicates that ITZ mixes with POPC in this concentration range. Increasing the ITZ concentration in the POPC monolayer causes the appearance of bright structures in the BAM images, and these persist up to the pressure of collapse. At higher ITZ concentrations, the features are very similar to those observed for the one-component ITZ film. This suggests that at higher concentrations, the interactions between POPC and ITZ are unfavorable, leading to phase separation with ITZ expelled from the POPC film. The presence of the PEGylated lipid causes the drug-POPC miscibility to be slightly reduced. However, the POPC/DSPE-PEG monolayer with 15 mol % of ITZ is still homogeneous at π = 30 mN/m, where the properties of lipid monolayers correlate with those of bilayers.[55]

3.2. Cryo-TEM Shows PEGylation of POPC Membranes under ITZ-Rich Conditions To Affect Liposome Size Distribution and Therefore Liposome Curvature and Stability. ITZ was incorporated into POPC and POPC/DSPE-PEG liposomes at a mole fraction of 0.15. The morphology of the ITZ-laden liposomes was directly visualized using cryo-TEM microscopy. Typical cryo-TEM micrographs are shown in Figure 7. For comparison, the morphology of pristine POPC liposomes is shown in Figure s3. The POPC SUVs are isolated vesicles with a clear spherical shape, and the unilamellar liposomes are the main population. It is found that embedding ITZ into the POPC membrane induces the formation of vesicle aggregates (Figure 7A). The aggregates are composed of individual liposomes that coalesce, and the contact area between the vesicles is clearly flattened. In addition, twinned or multilamellar vesicles form a significant part of the liposome population.

The cryo-TEM micrographs clearly showed that the incorporation of a hydrophobic drug into a lipid bilayer causes some instability of liposomal dispersions, resulting in an organization of small unilamellar vesicles into aggregated structures or fusion processes. On the contrary, for the sample containing the PEGylated liposomes (Figure 7B), well-separated unilamellar vesicles of spherical shape and distinct membrane enclosing an aqueous core were observed. Thus, solubilization of ITZ up to the content of 15 mol % in the PEGylated membrane did not disturb the process of liposome formation, and the vesicles with diameters lower than 85 nm were formed through sonication.

3.3. Fluorescence Quenching Measurements Indicate PEGylation To Have a Strong Effect on ITZ Binding Depth in the Membrane System. To estimate the

DOI: 10.1021/acs.molpharmaceut.6b00969
Mol. Pharmaceutics 2017, 14, 1057−1070

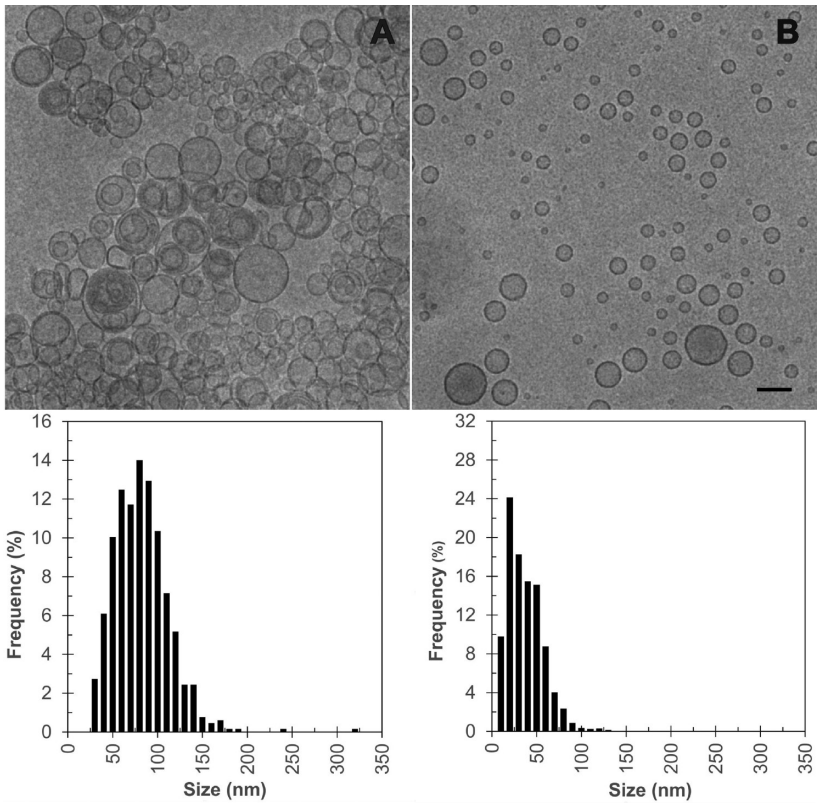

Figure 7. Cryo-TEM micrographs for (A) the POPC liposomes containing ITZ at a mole fraction equal to 0.15 and (B) the POPC/DSPE-PEG liposomes containing ITZ at a mole fraction equal to 0.15. The bar corresponds to 100 nm.

localization of ITZ in membranes, we performed fluorescence quenching experiments. KI was applied as an effective quencher of ITZ emission. Fluorescence quenching is frequently described by the Stern–Volmer equation:[56]

$$\frac{F_0}{F} = 1 + K_{SV}[Q] \quad (1)$$

where F_0 and F are intensities of dye fluorescence in absence and presence of the quencher, respectively, K_{SV} is a Stern–Volmer quenching constant, and [Q] is the concentration of quencher.

To determine the K_{SV} for ITZ incorporated in a lipid bilayer, we plotted the dependence F_0/F versus [Q] (Figure 8) and fitted to eq 1. The linear Stern–Volmer plots were obtained for both systems. The values of K_{SV} were 27.6 ± 1.6 M^{-1} and 166.9 ± 6.3 M^{-1} for ITZ solubilized in the pure POPC and PEGylated liposomes, respectively. Thus, fluorescence of ITZ embedded in both liposome types was quenched by I^-. The quenching efficiency of the anions was, however, different in the distinct lipid systems. In POPC liposomes, the extent of quenching was significantly reduced, indicating that the drug molecules were situated deeper in comparison to their position in the PEGylated liposomes. The value of K_{SV} for ITZ solubilized in the PEGylated liposomes is higher than that for ITZ embedded in the POPC liposomes, indicating that the drug molecules are probably partially embedded into the polymeric corona.

3.4. MD Simulations Highlight in Nanoscale How PEGylation Modulates ITZ Binding. *ITZ Has a Strong Driving Force To Enter the Bilayer and the PEGylated Layer.* We first used atomistic MD simulations to study the partitioning of ITZ through the lipid membrane, from the

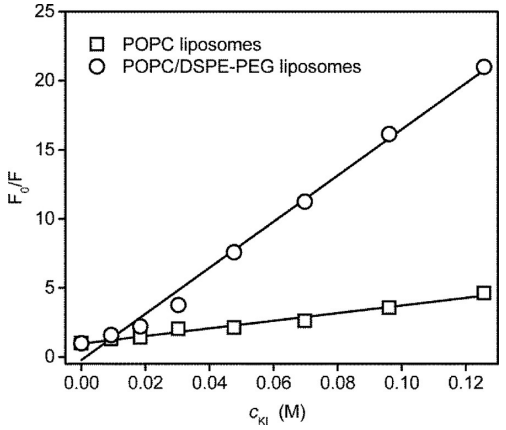

Figure 8. Stern–Volmer plots for fluorescence quenching of ITZ (c_{ITZ} = 1.8 μM) embedded in pristine POPC (squares) and POPC/DSPE-PEG (circles) membranes. KI was applied as the quencher.

aqueous phase to the membrane core. In the absence of PEGylation, we explored the dynamics of individual ITZ molecules interacting with a POPC bilayer (four replicas of system M1; Table 1). For the PEGylated membrane, we focused on system M5 composed of POPC and DSPE-PEG (two replicas; Table 1) together with six ITZ molecules initially placed in bulk water.

Figure 9A,B demonstrates how the ITZ molecules move in the systems along the bilayer normal (z-direction) during the simulations. Figure 9A depicts that all the ITZ molecules migrate into the POPC bilayer within 50 to 450 ns. Over the last 500 ns, ITZs reside in positions near the membrane polar region and do not display the tendency to translocate to the

DOI: 10.1021/acs.molpharmaceut.6b00969
Mol. Pharmaceutics 2017, 14, 1057–1070

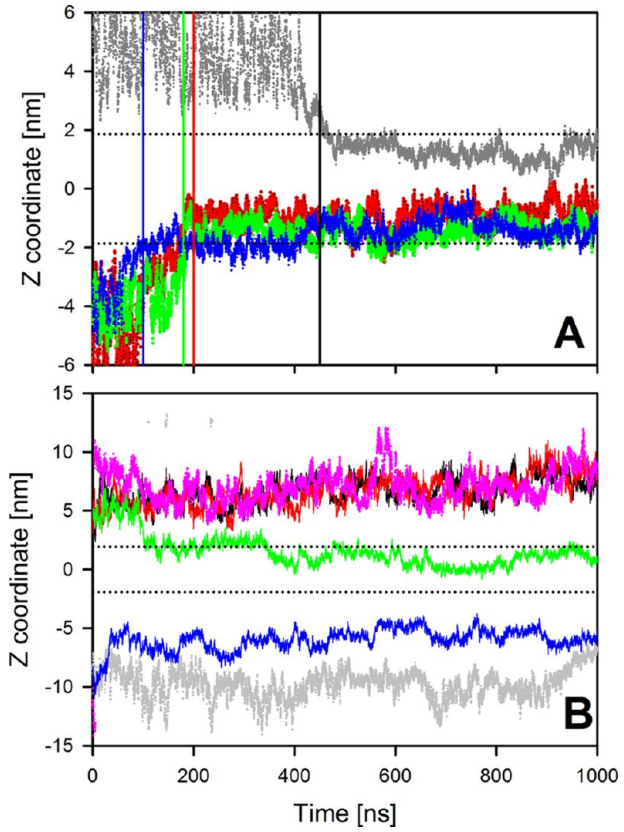

Figure 9. (A) Trajectories of the center of mass of ITZ based on four independent simulations of the POPC bilayer (system M1), where data for each simulation are shown with a different color. Vertical solid lines indicate the approximate time when the ITZ molecule entered the membrane, and horizontal dotted lines indicate the average position of the phosphorus atoms in the two membrane leaflets. (B) Trajectories of the ITZ center of mass in the POPC/DSPE-PEG bilayer (system M5, data for only single replica are presented for clarity).

other leaflet. Meanwhile, Figure 9B shows that in the PEGylated bilayer only two of the 12 ITZ molecules (altogether in the two replicas) enter the membrane and remain there for the remaining simulation time. Nevertheless, one ITZ molecule effectively enters the lipid bilayer and adopts a perpendicular orientation with respect to the bilayer normal. However, given the slow partitioning dynamics in the PEGylated system, the data do not allow one to draw conclusions about equilibrium partitioning between the PEG layer and the membrane.

ITZ Positions Itself to the PEG Layer or under the Lipid Head Groups. We next considered the effect of the ITZ concentration on ITZ location and arrangement in the non-PEGylated lipid bilayer. To this end, we investigated three additional systems (M2, M3, and M4; Table 1) containing different numbers of ITZ molecules initially immersed in the POPC membrane. Selected snapshots taken from the final frame of the simulations, illustrating the orientation and location of the ITZ molecules in the lipid bilayers are shown in Figure 3. It indicates that the preferred arrangement and position of ITZ can depend on the drug content in the membrane. To elucidate the ITZ location with respect to lipid molecules, we computed the mass density profiles across the membrane for the drug and selected lipid groups (Figure 10). Figure 10A,C,D,E show that regardless of the ITZ concentration in the POPC bilayer, the distribution of ITZ has a maximum at ∼1.0 nm from the bilayer center. This overlaps with the density profiles of glycerol and the double bond of POPC. The most favorable position of ITZ therefore lies between the glycerol backbones and the double bonds.

For system M5 containing the PEGylated lipids, two peaks in the density profile of ITZ can be observed (Figure 10B). One peak, at a distance of ∼1.0 nm, corresponds to ITZ located in the hydrocarbon core of the POPC/DSPE-PEG membrane. Another maximum is located at a distance of 4−5 nm from the bilayer center, therefore overlapping with the profile of PEG chains. This confirms that ITZ prefers to lie either (1) inside the membrane core or (2) within the PEG corona.

Next, we analyzed the distributions of the tilt angle for the systems containing the POPC membrane. Figure 11 shows the orientation of ITZ as a function of drug concentration. The molecules mostly adopt the orientation parallel to the bilayer surface. With an increasing drug content, a second peak appears at an angle of ∼25°, and the contribution of these molecules that are aligned parallel to the lipid acyl chains instead of being parallel to the membrane surface increases with ITZ concentration.

Hydrogen Bonds and Charge Pairs Involving ITZ Are Not Strongly Dependent on ITZ Concentration. To evaluate polar interactions of ITZ with water and lipids, we calculated the number of hydrogen bonds and charge pairs. A hydrogen bond was considered to be formed[57] when the acceptor−donor distance was ≤0.325 nm, and the angle between the acceptor−donor vector and the covalent donor−hydrogen bond was ≤35°. For charge pairs we used a criterion that the distance between the negatively charged ITZ atoms and the positively charged methyl substituents of the choline group was less than the distance cutoff of 0.4 nm (the cutoff distance is defined as the position of the first minimum in the relevant radial distribution functions).[58] These calculations were performed in the absence of PEGs for the systems M2, M3, and M4. The number of hydrogen bonds with water was found to be 2.8 ± 0.2 per ITZ molecule, which was found not to depend on the ITZ concentration. Meanwhile, the number of charge pairs was observed to decrease with increasing ITZ concentration from 1.0 ± 0.02 with 3 mol % to 0.81 ± 0.04 and 0.71 ± 0.02 with 9.1 mol % and 16.6 mol %, respectively.

ITZ Increases POPC Acyl Chain Order Right under Lipid Head Groups but Decreases the Order in the Membrane Center. The area per molecule (A_M) was calculated by dividing the total area of the simulation system by the number of POPC and ITZ molecules in a single bilayer leaflet, and the area per lipid (A_L) was then computed by dividing the total area of the simulation box by the number of POPC molecules in a single membrane leaflet (Table 2). The value for A_M is a more suitable for comparison with monolayer experiments, while A_L better describes the properties of the lipid bilayer. The thickness of the lipid membrane was estimated as a PP-distance: the distance between density maxima of phosphate groups in the opposite membrane leaflets. The area per POPC was 0.66 nm^2, in agreement with experimental data.[59] Increasing the ITZ concentration results in a slight decrease in A_M and an increase in A_L.

Next, we calculated the molecular order parameter, S_{CD}, defined as

$$S_{CD} = \left\langle \frac{3}{2}(\cos^2 \theta_i) - \frac{1}{2} \right\rangle \quad (2)$$

DOI: 10.1021/acs.molpharmaceut.6b00969
Mol. Pharmaceutics 2017, 14, 1057−1070

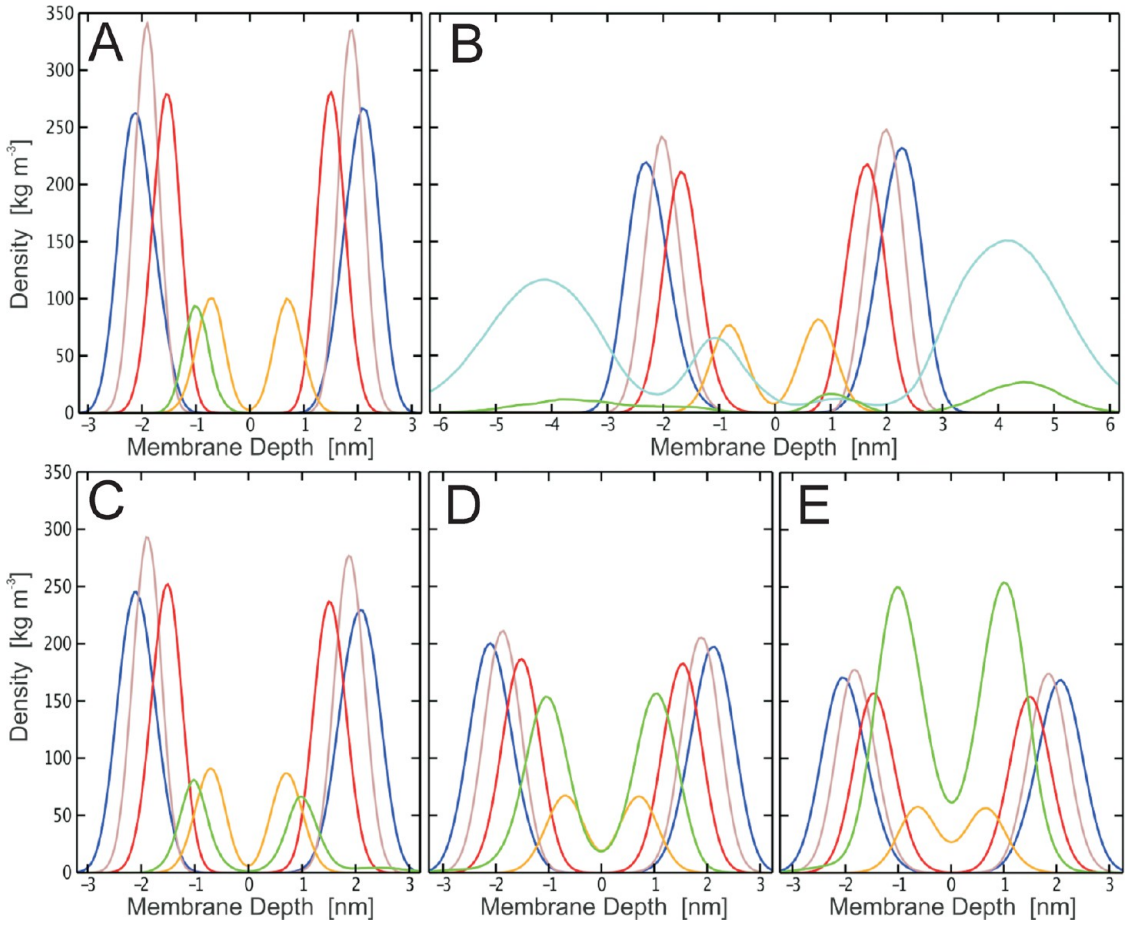

Figure 10. Mass density profiles of ITZ molecules (green lines) and selected lipid atoms along the bilayer normal direction as averaged over the last 250 ns of the trajectories in systems (A) M1, (B) M5, (C) M2, (D) M3, and (E) M4. The color code of lipids is as follows: blue (choline atoms), gray (phosphate atoms), red (glycerol and carbonyl backbone atoms), orange (double bonds atoms in POPC), and cyan (PEG chains). For clarity, the densities of ITZ (in panels A and B) were multiplied by two, and the densities of glycerol and carbonyl backbone were divided by two. A value of zero for membrane depth corresponds to membrane center.

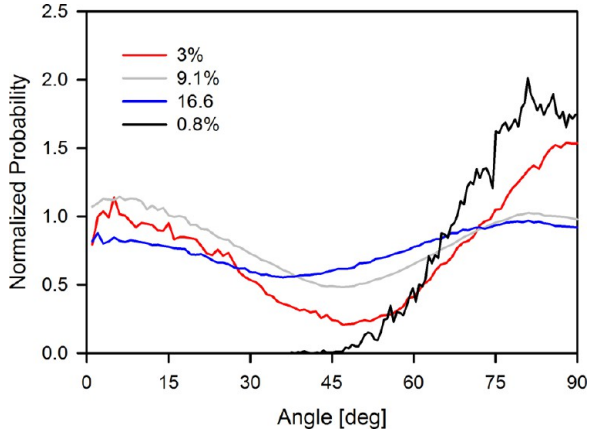

Figure 11. Distribution of the tilt angle between the ITZ long axis (see Figure 1) and the bilayer normal averaged over all replicas.

where θ_i is the angle between a C−D bond (C−H in simulations) of the i^{th} carbon atom and the bilayer normal. The angular brackets denote averaging over time and over relevant C−D bonds in the bilayer. The S_{CD} profiles along the POPC *sn*-1 acyl chain are shown in Figure 12. The profile obtained for the bilayer with 9.1 mol % concentration of ITZ is characterized by an increase in order in the beginning of the acyl chain, where ITZ molecules are located, while the order closer to the bilayer center and the core is not affected by ITZ. For the largest ITZ concentration (16.6 mol %), the first segments of acyl chains are more ordered than in the single-component lipid bilayer, but the segments below the seventh carbon atom are less ordered than in the pure POPC bilayer.

Table 2. Results for Surface Areas Per Molecule (A_M and A_L) and Bilayer Thickness[a]

system	concentration of ITZ	A_M (nm^2)	A_L (nm^2)	thickness (nm)
M0	0 mol %	0.66	0.66	3.60
M1	~0.8 mol %	0.66	0.66	3.80
M2	3.0 mol %	0.65	0.67	3.78
M3	9.1 mol %	0.646	0.71	3.74
M4	16.6 mol %	0.659	0.79	3.64
M5	1.2 mol %	0.623	0.63	4.18

[a]Error bars for the area per molecule are ±0.04 nm^2 and for membrane thickness ±0.05 nm.

4. DISCUSSION

In this paper, we showed data for the behavior of ITZ in the presence of a zwitterionic bilayer and a PEGylated membrane used for drug delivery purposes. Several aspects of the ITZ-membrane interactions were considered. The most important

DOI: 10.1021/acs.molpharmaceut.6b00969
Mol. Pharmaceutics 2017, 14, 1057−1070

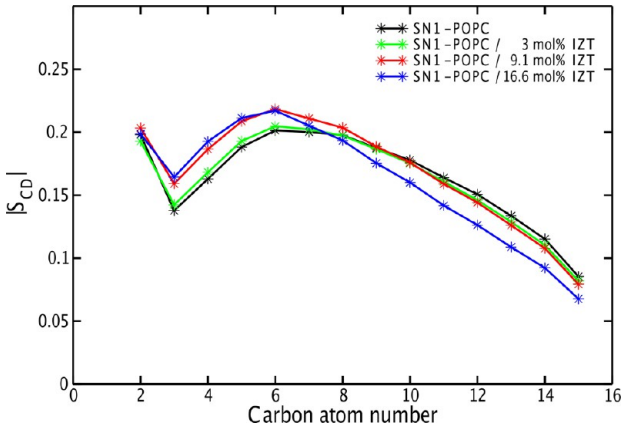

Figure 12. Profile of the S_{CD} order parameter for the *sn*-1 chain of POPC in a single-component POPC bilayer (black line) and in systems M2 (green line), M3 (red line), and M4 (blue line).

are (i) entry of hydrophobic ITZ to a lipid membrane; (ii) location, orientation, and translocation of this drug in a membrane; (iii) miscibility of ITZ in a lipid membrane; and (iv) the effect of the PEG corona at the lipid membrane surface on the migration of ITZ into a membrane and the subsequent final location of ITZ in the bilayer. In our studies, we used the PEGylated lipid with the polymer length of 45 units (a molecular weight of ∼2 kDa) because PEG is the most frequently used in pharmaceutical applications.[60] It is known that embedding more than 10 mol % of DSPE-PEG into a liposomal membrane leads to phase separation into PEG-poor liposomes and PEG-rich micelles.[61] Therefore, our computer simulations and experimental measurements were performed for systems with 7 mol % of PEGylated lipid in order to ensure that we were studying a system where phase separation would not occur.

ITZ is a weak basic drug with pK_as ≤ 4.0,[62] and thus, it is unionized at physiological pH. It was found experimentally that the neutral form of ITZ has very poor water-solubility.[5] Thus, ITZ molecules are mostly aggregated in aqueous solutions. For simulations, we therefore constructed systems containing the neutral form of ITZ, taking into account the acid−base equilibrium of ITZ in the aqueous medium. We observed the aggregation process in simulations with four ITZ molecules initially located in bulk water. On the other hand, the presence of the PEG layer at the membrane surface reduced the aggregation of ITZ. Because both ITZ aggregation and its interactions with PEG are driven by contact between hydrophobic surfaces, one can assume that there is a competition between these interactions. Thus, increasing interaction of ITZ with PEG is expected to diminish its aggregation (see below). This is in line with our previous result that an increase in PEG concentration results in a decrease in hematoporphyrin aggregation.[63]

Generally, the entry of small organic molecules into lipid bilayers is relatively poorly understood. This aspect of the guest molecule−membrane interactions is accessible mostly by computer simulations. While there is a large number of MD simulation studies on various organic compound-lipid bilayer systems,[64−66] the entry of guest molecules to a bilayer has not attracted much attention, probably due to the long time scale of this self-assembly process.[67] In this study, we carried out a set of 1 μs long simulations to visualize the entry of ITZ into lipid membranes with and without PEGylation. The overall process of ITZ entering a membrane is depicted in Figure 2. Because the number of observed events is limited, we can describe the partitioning process only qualitatively.

ITZ has an elongated shape with two different groups at its ends: 1-methylpropyl and dichlorophenyl. In all cases we studied, ITZ aligned itself almost parallel to the lipid chains before entering the membrane with one of these groups leading. When ITZ was inside the membrane, the molecule changed its orientation to lie parallel to the surface at a distance of 1.0 nm from the membrane center (between glycerol and the double bond of POPC). A small subset of ITZ molecules, however, aligned at a tilt angle of ∼25° at higher concentrations. At first sight such an orientation and location might look unreasonable given that this is the most ordered and rigid region of the membrane. However, the parallel arrangement of ITZ in the POPC membrane can be justified by the chemical structure of the drug and its interactions with water and the polar groups of POPC. First, ITZ is partially hydrated by about 2.8 water molecules. Second, ITZ contains several electronegative atoms: 8 nitrogens, 4 oxygens, and 2 chlorines that are regularly distributed along the molecular skeleton. These atoms have relatively high partial charges up to −0.61 e and the interactions between them and the polar lipid headgroups is expected. As all polar groups of ITZ and lipids are hydrogen acceptors, there are no direct hydrogen bonds between them, but instead, the interactions between ITZ and the choline groups are based on electrostatics. Given these points, the adopted orientation of ITZ is quite optimal because it is stabilized by hydrogen bonds with water and polar interactions between lipid head groups and the electronegative atoms of ITZ. Additionally, the degree of contact between the hydrophobic groups of ITZ and water is reduced. The transverse arrangement of ITZ in the POPC bilayer had a clear effect on membrane properties, especially on the area per lipid (A_L). For pure POPC, this parameter was ∼0.66 nm^2 and increased considerably with increasing ITZ concentration (Table 2). ITZ increased the ordering of the upper segments of the acyl chains but decreased the order in the lower half of the chains closer to their terminal carbon.

In Figure 10B we see that our result for the mass density profile shows that the density of PEG has two maxima: one located outside the bilayer, with the peak at a distance of ∼4.2 nm from the membrane center, and a second density peak inside the membrane with a peak at a position of about 1.1 nm from the membrane center. This result, in agreement with our previous published results,[28,68] demonstrates that PEG can penetrate into the membrane interior and will thus affect the membrane properties.

Our simulation results demonstrate that the effect of the presence of PEG on the membrane properties in turn effects the arrangement of ITZ within the lipid membrane. The ITZ molecules were seen to locate both within the membrane, at a distance of ∼1.0 nm from the membrane center, and within the PEG layer at a distance of ∼4.4 nm from the membrane center. The orientation of the ITZ molecules, within the membrane, parallel to the membrane surface, was unchanged by the presence of PEG. The presence of ITZ within the PEG layer results from known properties of PEG, which is known to be soluble in both polar and nonpolar media; PEG is not completely hydrophobic,[63,69,70] and thus, the interaction with ITZ is a lipophilic interaction between the nonpolar $(CH_2)_2$ groups of the PEG chain and the nonpolar molecular surface.[63] As a highly lipophilic molecule, with a lipophilicity parameter,

DOI: 10.1021/acs.molpharmaceut.6b00969
Mol. Pharmaceutics 2017, 14, 1057−1070

log *P*, of 6.2, such a lipophilic interaction is to be expected for ITZ. As a result, the PEG chains densely wrap around the ITZ molecules, as we have observed in a previous study of the interaction between PEG and hydrophobic porphyns.[69] This effect is noteworthy regarding the role of PEGylation in the LDS; this effect could slow down drug release.

Our computational results can be validated by the fluorescence quenching measurements. In the case of pristine POPC membranes, the quenching efficiency by the iodide ions is relatively low. This indicates that ITZ molecules are embedded into the POPC membrane, and thus, their accessibility to the quencher is reduced. Judging from the K_{SV} values, the quenching process of the drug incorporated into PEGylated liposomes was 6 times more effective compared to that in the system with conventional liposomes. Thus, a part of the ITZ molecules were located outside the membrane and more accessible to the quencher. Therefore, the findings from the quenching experiments strongly support the results of our atomistic MD simulations, indicating that in the presence of PEGylated lipid, the drug has a preferred location within the PEG layer.

The monolayer experiments, performed at the physiologically relevant pH of 7.4 at 37 °C, revealed that approximately 15 mol % of ITZ can be incorporated into both conventional and PEGylated membranes without phase separation of the drug. Our MD simulations are in line with this observation (see Table 2). Figure S4 shows top views of the POPC membranes containing 9.1 and 16.6 mol % of ITZ. While at the lower concentration the ITZ molecules are well separated by lipids, at the higher concentration some ITZ molecules aligned parallel to each other, indicating that dimers or higher aggregates were formed. However, no ITZ-rich domains were observed.

Finally, cryo-TEM observation clearly showed that the conventional liposomes aggregated after incorporation of 15 mol % of ITZ. However, the aggregates consisted of individual distinctive liposomes that stick to each other. This likely resulted from the modification of bilayer properties by a more superficial location of ITZ at this concentration as shown in the MD simulations. Figure 10E shows that the density profile of ITZ at 16.6 mol % partially overlapped with the profiles of lipid phosphates and choline molecules. This indicates that because of large drug content, a part of the ITZ molecules was embedded in the membrane headgroup region. The incorporation of PEGylated lipids prevents aggregation and favors liposomes of smaller size in comparison to conventional liposomes.

5. CONCLUSIONS

We performed a synergistic combination of computational and experimental analysis on interactions of PEGylated and non-PEGylated membranes with an important antifungal agent, ITZ, in order to obtain mechanistic insight relevant to ITZ delivery via liposome based delivery systems. Our results showed superiority of PEGylated liposomes over conventional ones as carriers of ITZ. First, all cryo-TEM micrographs demonstrated that conventional liposomes loaded with ITZ tend to aggregate, rendering them less stable. This behavior observed in conventional liposomes seems to correlate with changes in the structural properties of the lipid membrane induced by ITZ insertion.

Our studies also indicated that in PEGylated bilayers ITZ locates inside the lipid bilayer in a fashion similar to that observed with non-PEGylated lipids; however, ITZ was observed also within the PEG layer. This prediction given by atomistic simulations was validated by fluorescence quenching experiments. It is therefore quite plausible that PEGylated liposomes have a capacity to adsorb a larger amount of ITZ. Future studies considering the payload of PEGylated liposomes will likely clarify this issue.

The current study represents a continuation of our work based on a synergistic combination of experimental and computational methodologies. The aim is to obtain mechanistic insight into the rational design of LDS-based drug delivery systems possible. While PEG is currently the gold standard, there is room for improvement and a rational design process requires a mechanistic understanding of the behavior of PEG to provide a foundation of knowledge for this research.[17,18]

■ ASSOCIATED CONTENT

Supporting Information

The Supporting Information is available free of charge on the ACS Publications website at DOI: 10.1021/acs.molpharmaceut.6b00969.

Partial charges at ITZ molecule, additional figures, and topology in GROMACS format of ITZ molecule (PDF)

■ AUTHOR INFORMATION

Corresponding Authors

*E-mail for M.K.: kepczyns@chemia.uj.edu.pl. Tel.: +48 12 6632020. Fax: +48 12 6340515.

*E-mail for T.R.: tomasz.rog@gmail.com. Tel.: +358 40 198 1010.

ORCID

Ilpo Vattulainen: 0000-0001-7408-3214

Mariusz Kepczynski: 0000-0002-7304-6881

Tomasz Róg: 0000-0001-6765-7013

Author Contributions

‖(M.D.-R. and C.P.) These authors contributed equally.

Notes

The authors declare no competing financial interest.

■ ACKNOWLEDGMENTS

This project was financed by the National Science Centre Poland on the basis of the decision number DEC-2012/07/B/ST5/00913. TR, AB, CP, and IV acknowledge the Academy of Finland (Center of Excellence program) and the European Research Council (Advanced Grant CROWDED-PRO-LIP-IDS). JB acknowledges support from the Grant Agency of the Czech Republic (P302/12/G157) and Charles University in Prague (PRVOUK P27/LF1/1 and UNCE 204022). For computational resources, we wish to thank CSC − IT Centre for Science Ltd.

■ REFERENCES

(1) Grant, S. M.; Clissold, S. P. Itraconazole. A Review of its Pharmacodynamic and Pharmacokinetic Properties and Therapeutic Use in Superficial and Systemic Mycoses. *Drugs* **1989**, *37*, 310−344.

(2) Van Cauteren, H.; Heykants, J.; De Coster, R.; Cauwenbergh, G. Itraconazole: Pharmacologic Studies in Animals and Humans. *Clin. Infect. Dis.* **1987**, *9*, S43−S46.

(3) Hostetler, J. S.; Heykants, J.; Clemons, K. V.; Woestenborghs, R.; Hanson, L. H.; Stevens, D. A. Discrepancies in bioassay and chromatography determinations explained by metabolism of itraconazole to hydroxyitraconazole: studies of interpatient variations in concentrations. *Antimicrob. Agents Chemother.* **1993**, *37*, 2224−2227.

(4) Tapaninen, T.; Backman, J. T.; Kurkinen, K.; Neuvonen, P. J.; Niemi, M. Itraconazole, a P-Glycoprotein and CYP3A4 Inhibitor, Markedly Raises the Plasma Concentrations and Enhances the Renin-Inhibiting Effect of Aliskiren. *J. Clin. Pharmacol.* **2011**, *51*, 359−367.
(5) Peeters, J.; Neeskens, P.; Tollenaere, J. P.; Van Remoortere, P.; Brewster, M. E. Characterization of the interaction of 2-hydroxypropyl-β-cyclodextrin with itraconazole at pH 2, 4 and 7. *J. Pharm. Sci.* **2002**, *91*, 1414−1422.
(6) Lee, S. Y.; Jung, I. I.; Kim, J. K.; Lim, G. B.; Ryu, J. H. Preparation of itraconazole/HP-β-CD inclusion complexes using supercritical aerosol solvent extraction system and their dissolution characteristics. *J. Supercrit. Fluids* **2008**, *44*, 400−408.
(7) Groll, A. H.; Wood, L.; Roden, M.; Mickiene, D.; Chiou, C. C.; Townley, E.; Dad, L.; Piscitelli, S. C.; Walsh, T. J. Safety, Pharmacokinetics and Pharmacodynamics of Cyclodextrin Itraconazole in Pediatric Patients with Oropharyngeal Candidiasis. *Antimicrob. Agents Chemother.* **2002**, *46*, 2554−2563.
(8) Jung, J. Y.; Yoo, S. D.; Lee, S. H.; Kim, K. H.; Yoon, D. S.; Lee, K. H. Enhanced solubility and dissolution rates of itraconazole by a solid dispersion technique. *Int. J. Pharm.* **1999**, *187*, 209−218.
(9) Akkar, A.; Muller, R. H. Intravenous itraconazole emulsions produced by SolEmuls technology. *Eur. J. Pharm. Biopharm.* **2003**, *56*, 29−36.
(10) Baert, L. E. C.; Peeters, J.; Verreck, G.; Jassen Pharmaceutica NV. Solid mixtures of cyclodextrins prepared via melt-extrusion. U.S. Patent US6365188B1, April 4, 2002.
(11) Gillis, P. M. V.; Victor De, C. V. F.; Vandecruys, R. P. G.; Jassen Pharmaceutica NV. Beads having a core coated with an antifungal and a polymer. World Patent WO 94/05263, Mar. 17, 1994.
(12) Rhee, Y. S.; Park, C. W.; Nam, T. Y.; Shin, Y. S.; Chi, S. C.; Park, E. S. Formulation of Parenteral Microemulsion Containing Itraconazole. *Arch. Pharmacal Res.* **2007**, *30*, 114−123.
(13) PDR Staff Medical Economics. *Physicians' Desk Reference*, 59th ed., Thomson PDR: Montvale, NJ, 2005; pp 1757−1766.
(14) van Balen, G. P.; Martinet, C. a. M.; Caron, G.; Bouchard, G.; Reist, M.; Carrupt, P. A.; Fruttero, R.; Gasco, A.; Testa, B. Liposome/Water Lipophilicity: Methods, Information Content, and Pharmaceutical Applications. *Med. Res. Rev.* **2004**, *24*, 299−324.
(15) Kępczyński, M.; Pandian, R. P.; Smith, K. M.; Ehrenberg, B. Do Liposome-binding Constants of Porphyrins Correlate with Their Measured and Predicted Partitioning Between Octanol and Water? *Photochem. Photobiol.* **2002**, *76*, 127−134.
(16) Lasic, D. D. Novel applications of liposomes. *Trends Biotechnol.* **1998**, *16*, 307−321.
(17) Bunker, A.; Magarkar, A.; Viitala, T. Rational design of liposomal drug delivery systems, a review: Combined experimental and computational studies of lipid membranes, liposomes and their PEGylation. *Biochim. Biophys. Acta, Biomembr.* **2016**, *1858*, 2334−2352.
(18) Kepczynski, M.; Róg, T. Functionalized lipids and surfactants for specific applications. *Biochim. Biophys. Acta, Biomembr.* **2016**, *1858*, 2362−2379.
(19) Kohli, A. G.; Kierstead, P. H.; Venditto, V. J.; Walsh, C. L.; Szoka, F. C. Designer lipids for drug delivery: From heads to tails. *J. Controlled Release* **2014**, *190*, 274−287.
(20) Ali, M. H.; Moghaddam, B.; Kirby, D. J.; Mohammed, A. R.; Perrie, Y. The role of lipid geometry in designing liposomes for the solubilisation of poorly water soluble drugs. *Int. J. Pharm.* **2013**, *453*, 225−232.
(21) Eloy, J. O.; Claro de Souza, M.; Petrilli, R.; Barcellos, J. P. A.; Lee, R. J.; Marchetti, J. M. Liposomes as carriers of hydrophilic small molecule drugs: strategies to enhance encapsulation and delivery. *Colloids Surf., B* **2014**, *123*, 345−363.
(22) Chow, A.; Brown, B. D.; Merad, M. Studying the mononuclear phagocyte system in the molecular age. *Nat. Rev. Immunol.* **2011**, *11*, 788−798.
(23) Yan, X.; Scherphof, G. L.; Kamps, J. A. A. M. Liposome opsonization. *J. Liposome Res.* **2005**, *15*, 109−139.
(24) Moghimi, S. M.; Szebeni, J. Stealth liposomes and long circulating nanoparticles: critical issues in pharmacokinetics, opsonization and protein-binding properties. *Prog. Lipid Res.* **2003**, *42*, 463−478.
(25) Romberg, B.; Oussoren, C.; Snel, C. J.; Carstens, M. G.; Hennink, W. E.; Storm, G. Pharmacokinetics of poly(hydroxyethyl-l-asparagine)- coated liposomes is superior over that of PEG-coated liposomes at low lipid dose and upon repeated administration. *Biochim. Biophys. Acta, Biomembr.* **2007**, *1768*, 737−743.
(26) Woodle, M. C. Controlling liposome blood clearance by surface-grafted polymers. *Adv. Drug Delivery Rev.* **1998**, *32*, 139−152.
(27) Dinç, C. O.; Kibarer, G.; Güner, A. Solubility profiles of poly(ethylene glycol)/solvent systems. II. comparison of thermodynamic parameters from viscosity measurements. *J. Appl. Polym. Sci.* **2010**, *117*, 1100−1119.
(28) Stepniewski, M.; Pasenkiewicz-Gierula, M.; Róg, T.; Danne, R.; Orlowski, A.; Karttunen, M.; Urtti, A.; Yliperttula, M.; Vuorimaa, E.; Bunker, A. Study of PEGylated Lipid Layers as a Model for PEGylated Liposome Surfaces: Molecular Dynamics Simulation and Langmuir Monolayer Studies. *Langmuir* **2011**, *27*, 7788−7798.
(29) Curic, A.; Reul, R.; Möschwitzer, J.; Fricker, G. Formulation optimization of itraconazole loaded PEGylated liposomes for parenteral administration by using design of experiments. *Int. J. Pharm.* **2013**, *448*, 189−197.
(30) Le Conte, P.; Joly, V.; Saint-Julien, L.; Gillardin, J. M.; Carbon, C.; Yeni, P. Tissue Distribution and Antifungal Effect of Liposomal Itraconazole in Experimental Cryptococcosis and Pulmonary Aspergillosis. *Am. Rev. Respir. Dis.* **1992**, *145*, 424−429.
(31) Wang, J.; Huang, G. Preparation of itraconazole-loaded liposomes coated by carboxymethyl chitosan and its pharmacokinetics and tissue distribution. *Drug Delivery* **2011**, *18*, 631−638.
(32) Magarkar, A.; Róg, T.; Bunker, A. Molecular Dynamics Simulation of PEGylated Membranes with Cholesterol: Building Toward the DOXIL Formulation. *J. Phys. Chem. C* **2014**, *118*, 15541−15549.
(33) Magarkar, A.; Róg, T.; Bunker, A. Molecular dynamics simulation of inverse-phosphocholine lipids. *J. Phys. Chem. C* **2014**, *118*, 19444−19449.
(34) Magarkar, A.; Karakas, E.; Stepniewski, M.; Róg, T.; Bunker, A. Molecular dynamics simulation of PEGylated bilayer interacting with salt ions: a model of the liposome surface in the bloodstream. *J. Phys. Chem. B* **2012**, *116*, 4212−4219.
(35) Lehtinen, J.; Magarkar, A.; Stepniewski, M.; Hakola, S.; Bergman, M.; Róg, T.; Yliperttula, M.; Urtti, A.; Bunker, A. Analysis of cause of failure of new targeting peptide in PEGylated liposome: Molecular modeling as rational design tool for nanomedicine. *Eur. J. Pharm. Sci.* **2012**, *46*, 121−130.
(36) Kepczynski, M.; Bednar, J.; Kuzmicz, D.; Wydro, P.; Nowakowska, M. Spontaneous Formation of Densely Stacked Multilamellar Vesicles in Dioctadecyldimethylammonium Bromide/Oleosiloxane Mixtures. *Langmuir* **2010**, *26*, 1551−1556.
(37) Kepczynski, M.; Kumorek, M.; Stepniewski, M.; Róg, T.; Kozik, B.; Jamróz, D.; Bednar, J.; Nowakowska, M. Behavior of 2,6-Bis(decyloxy)naphthalene Inside Lipid Bilayer. *J. Phys. Chem. B* **2010**, *114*, 15483−15494.
(38) Kunze, K. L.; Nelson, W. L.; Kharasch, E. D.; Thummel, K. E.; Isoherranen, N. Stereochemical Aspects of Itraconazole Metabolism In Vitro and In Vivo. *Drug Metab. Dispos.* **2006**, *34*, 583−590.
(39) Jorgensen, W. L.; Maxwell, D. S.; Tirado-Rives, J. Development and Testing of the OPLS All-Atom Force Field on Conformational Energetics and Properties of Organic Liquids. *J. Am. Chem. Soc.* **1996**, *118*, 11225−11236.
(40) Maciejewski, A.; Pasenkiewicz-Gierula, M.; Cramariuc, O.; Vattulainen, I.; Róg, T. Refined OPLS−AA force field for saturated phosphatidylcholine bilayers at full hydration. *J. Phys. Chem. B* **2014**, *118*, 4571−4581.
(41) Kulig, W.; Pasenkiewicz-Gierula, M.; Róg, T. Topologies, structures and parameter files for lipid simulations in GROMACS with

DOI: 10.1021/acs.molpharmaceut.6b00969
Mol. Pharmaceutics 2017, 14, 1057−1070

the OPLS-aa force field: DPPC, POPC, DOPC, PEPC, and cholesterol. *Data in Brief* **2015**, *5*, 333−336.
(42) Kulig, W.; Pasenkiewicz-Gierula, M.; Róg, T. Cholesterol interactions with *Cis* and *Trans* unsaturated phosphatidylcholines. Molecular dynamics simulation study. *Chem. Phys. Lipids* **2016**, *195*, 12−20.
(43) Jorgensen, W. L.; Chandrasekhar, J.; Madura, J. D.; Impey, R. W.; Klein, M. L. Comparison of simple potential functions for simulating liquid water. *J. Chem. Phys.* **1983**, *79*, 926−935.
(44) Frisch, M. J.; Trucks, G. W.; Schlegel, H. B.; Scuseria, G. E.; Robb, M. A.; Cheeseman, J. R.; Montgomery, J. A., Jr.; Vreven, T.; Kudin, K. N.; Burant, J. C.; et al. *Gaussian 03*, revision C.02; Gaussian, Inc.: Wallingford, CT, 2004.
(45) Bayly, C. I.; Cieplak, P.; Cornell, W.; Kollman, P. A. A Well-Behaved Electrostatic Potential Based Method Using Charge Restraints for Deriving Atomic Charges: The RESP Model. *J. Phys. Chem.* **1993**, *97*, 10269−10280.
(46) Ribeiro, A. A. S. T.; Horta, B. A. C.; de Alencastro, R. B. MKTOP: a Program for Automatic Construction of Molecular Topologies. *J. Braz. Chem. Soc.* **2008**, *19*, 1433−1435.
(47) Bussi, G.; Donadio, D.; Parrinello, M. Canonical sampling through velocity rescaling. *J. Chem. Phys.* **2007**, *126*, 014101.
(48) Parrinello, M.; Rahman, A. Polymorphic transitions in single crystals: A new molecular dynamics method. *J. Appl. Phys.* **1981**, *52*, 7182−7190.
(49) Darden, T.; York, D.; Pedersen, L. Particle mesh Ewald: An NŸlog(N) method for Ewald sums in large systems. *J. Chem. Phys.* **1993**, *98*, 10089−10092.
(50) Hess, B.; Bekker, H.; Berendsen, H. J. C.; Fraaije, J. G. E. M. LINCS: A linear constraint solver for molecular simulations. *J. Comput. Chem.* **1997**, *18*, 1463−1472.
(51) Hess, B.; Kutzner, C.; van der Spoel, D.; Lindahl, E. GROMACS 4: Algorithms for highly efficient, load-balanced, and scalable molecular simulation. *J. Chem. Theory Comput.* **2008**, *4*, 435−447.
(52) Humphrey, W.; Dalke, A.; Schulten, K. VMD: visual molecular dynamics. *J. Mol. Graphics* **1996**, *14*, 33−38.
(53) Lozano, M. M.; Longo, M. L. Complex formation and other phase transformations mapped in saturated phosphatidylcholine/DSPE-PEG2000 monolayers. *Soft Matter* **2009**, *5*, 1822−1834.
(54) Inglot, K.; Martyński, T.; Bauman, D. Molecular organization and aggregation in Langmuir and Langmuir-Blodgett films of azo dye/liquid crystal mixtures. *Opto-Electron. Rev.* **2009**, *17*, 120−128.
(55) Kwolek, U.; Kulig, W.; Wydro, P.; Nowakowska, M.; Róg, T.; Kepczynski, M. Effect of Phosphatidic Acid on Biomembrane: Experimental and Molecular Dynamics Simulations Study. *J. Phys. Chem. B* **2015**, *119*, 10042−10051.
(56) Lakowicz, J. R. *Principles of Fluorescence Spectroscopy*; Plenum Press: New York, 1983.
(57) Murzyn, K.; Zhao, W.; Karttunen, M.; Kurdziel, M.; Róg, T. Dynamics of water at membrane surfaces: Effect of headgroup structure. *Biointerphases* **2006**, *1*, 98−105.
(58) Murzyn, K.; Róg, T.; Jezierski, G.; Takaoka, Y.; Pasenkiewicz-Gierula, M. Effects of phospholipid unsaturation on the membrane/water interface: a molecular simulation study. *Biophys. J.* **2001**, *81*, 170−183.
(59) Kucerka, N.; Nieh, M. P.; Katsaras, J. Fluid phase lipid areas and bilayer thicknesses of commonly used phosphatidylcholines as a function of temperature. *Biochim. Biophys. Acta, Biomembr.* **2011**, *1808*, 2761−2771.
(60) Maruyama, K.; Yuda, T.; Okamoto, A.; Ishikura, C.; Kojima, S.; Iwatsuru, M. Effect of Molecular Weight in Amphipathic Polyethyleneglycol on Prolonging the Circulation Time of Large Unilamellar Liposomes. *Chem. Pharm. Bull.* **1991**, *39*, 1620−1622.
(61) Ueno, M.; Sriwongsitanont, S. Effect of PEG Lipid on Fusion and Fission of Phospholipid Vesicles in the Process of Freeze-Thawing. *Polymer* **2005**, *46*, 1257−1267.
(62) Buchanan, C. M.; Buchanan, N.; Edgar, K. J.; Klein, S.; Little, J. L.; Ramsey, M. G.; Ruble, K. M.; Wacher, V. J.; Wempe, M. F. Pharmacokinetics of Itraconazole After Intravenous and Oral Dosing of Itraconazole-Cyclodextrin Formulations. *J. Pharm. Sci.* **2007**, *96*, 3100−3116.
(63) Li, Y.-C.; Rissanen, S.; Stepniewski, M.; Cramariuc, O.; Rog, T.; Mirza, S.; Xhaard, H.; Wytrwal, M.; Kepczynski, M.; Bunker, A. Study of Interaction between PEG Carrier and 3 Relevant Drug Molecules: Piroxicam, Paclitaxel, and Hematoporphyrin. *J. Phys. Chem. B* **2012**, *116*, 7334−7341.
(64) Postila, P. A.; Vattulainen, I.; Róg, T. Selective effect of synaptic membrane on neurotransmission. *Sci. Rep.* **2016**, *6*, 19345.
(65) Cramariuc, O.; Róg, T.; Javanainen, M.; Monticelli, L.; Polishchuk, A. V.; Vattulainen, I. Molecular dynamics simulations suggest a mechanism for translocation of fluoroquinolones across lipid membranes. *Biochim. Biophys. Acta, Biomembr.* **2012**, *1818*, 2563−2571.
(66) Cramariuc, O.; Róg, T.; Vattulainen, I. Drug−lipid membrane interaction mechanisms revealed through molecular simulations. *Curr. Phys. Chem.* **2012**, *2*, 379−400.
(67) Rissanen, S.; Kumorek, M.; Martinez-Seara, H.; Li, Y.−C.; Jamróz, D.; Bunker, A.; Nowakowska, M.; Vattulainen, I.; Kepczynski, M.; Róg, T. Effect of PEGylation on Drug Entry into Lipid Bilayer. *J. Phys. Chem. B* **2014**, *118*, 144−151.
(68) Dzieciuch, M.; Rissanen, S.; Szydłowska, N.; Bunker, A.; Kumorek, M.; Jamroz, D.; Vattulainen, I.; Nowakowska, M.; Rog, T.; Kepczynski, M. PEGylated Liposomes as Carriers of Hydrophobic Porphyrins. *J. Phys. Chem. B* **2015**, *119*, 6646−6657.
(69) Stępniewski, M.; Kepczynski, M.; Jamroz, D.; Nowakowska, M.; Rissanen, S.; Vattulainen, I.; Rog, T. Interaction of Hematoporphyrin with Lipid Membranes. *J. Phys. Chem. B* **2012**, *116*, 4889−4897.
(70) Lajunen, T.; Kontturi, L.-S.; Viitala, L.; Manna, M.; Cramariuc, O.; Róg, T.; Bunker, A.; Laaksonen, T.; Viitala, T.; Murtomäki, L.; Urtti, A. Indocyanine Green-Loaded Liposomes for Light-Triggered Drug Release. *Mol. Pharmaceutics* **2016**, *13*, 2095−2107.

DOI: 10.1021/acs.molpharmaceut.6b00969
Mol. Pharmaceutics 2017, 14, 1057−1070